*Reprinted from* **WAVES'97:** *Proceedings of the Third International Symposium on Ocean Wave Measurement and Analysis, Virginia Beach, VA – Nov. 3-7, 1997*

# Experimental Modeling of a Rip Current System

**Merrick C. Haller, R. A. Dalrymple, and I. A. Svendsen** [1]

## Abstract

Results from an experimental investigation of a rip current system in a laboratory wave basin are presented. The modeled system includes a planar beach with a superimposed longshore bar containing two rip channels. Dense measurements of water surface elevation, cross-shore and longshore currents are presented. The experimental results indicate that, in addition to the steady mean water level gradients which drive the steady nearshore circulation, time varying pressure gradients are generated in the rip current system and these gradients are directly related to measured current oscillations in the rips. Oscillations in the rip currents are shown to have multiple scales. A simple calculation shows that classical jet instability theory can predict the order of magnitude of the measured short time scale rip current oscillations.

## Background

Shepard (1936) first introduced the concept of the rip current. In the observations of Shepard et al. (1941) and Shepard and Inman (1950) those authors described three characteristics of rip currents: 1) they are driven by longshore variations in wave height 2) they exhibit periodic fluctuations in time and are often periodically spaced in the longshore direction and 3) they increase in strength with increasing wave height. Later observers also noted that many rip currents are not stationary (McKenzie, 1958; Short, 1985). The offshore end of the rips (the rip head) can flop around like an untended garden hose and the entire rip current can migrate in the longshore direction.

One commonly observed mechanism of rip current generation is nearshore wave height variations induced by longshore varying bottom bathymetry. In this paper we will investigate, in the laboratory, the waves and currents generated in a nearshore system characterized by a longshore varying bathymetry

[1]all at: Center for Applied Coastal Research, Ocean Engineering Lab, University of Delaware, Newark, DE 19716, USA. Correspondence e-mail: merrick@coastal.udel.edu

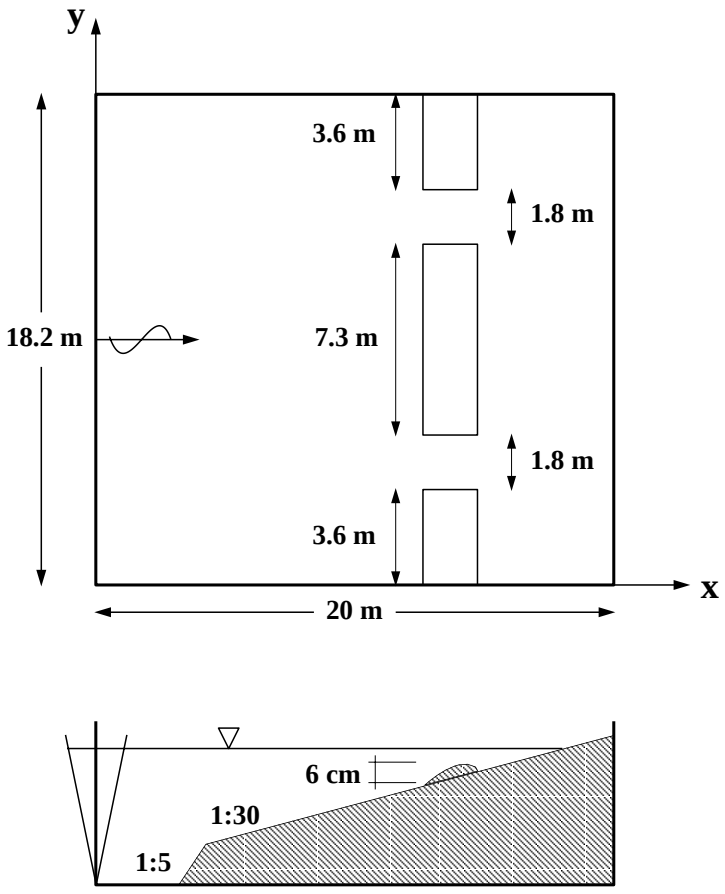


Figure 1: Plan view and cross-section of the experimental basin.

and periodic rip currents. A limited set of field measurements of rip current systems does exist (Sonu, 1972; Bowman *et al.*, 1988; Tang and Dalrymple, 1989), however, due to their transient nature rip currents tend to elude field investigators intent on measuring them with stationary instrument deployments. In contrast, the laboratory has proven to be very conducive to the study of rip currents since the environment is more easily controlled. Preliminary results from this experiment were given in Haller et al. (1996, 1997), the present work utilizes all the data obtained during this experiment therefore providing more detailed rip current measurements than reported previously and provides an in-depth discussion of the low frequency motion observed.

## Physical Model

The experiment was conducted in the 20m $\times$ 20m directional wave basin at the Center for Applied Coastal Research at the University of Delaware. The basin (Figure 1) contains a planar concrete beach of 1:30 slope, along with a steeper (1:5) toe structure. A discontinuous longshore bar made of molded

plastic was attached directly onto the beach slope. The crest of the bar is 6 cm above the planar beach and it has a parabolic shape in the cross-shore. The discontinuities result from the two gaps in the bar which act as rip channels and tend to fix the location of offshore directed rip currents depending on the wave conditions. These rip channels are located at 1/4 and 3/4 of the width of the basin and are each 1.8 m wide with sloped sides.

Separate arrays of ten capacitance wave gages and 3 acoustic-doppler velocity meters (ADV) were used to measure the generated wave fields, mean water levels ($\overline{\eta}$), and circulation patterns ($\vec{u} = (u, v)$). Details of the experimental procedure can be found in Haller et al. (1997). Most of the experimental runs lasted for $\sim 27$ minutes after the onset of wave generation. However a limited set of additional tests were conducted with longer runs of $\sim 45$ minutes and these will also be discussed here.

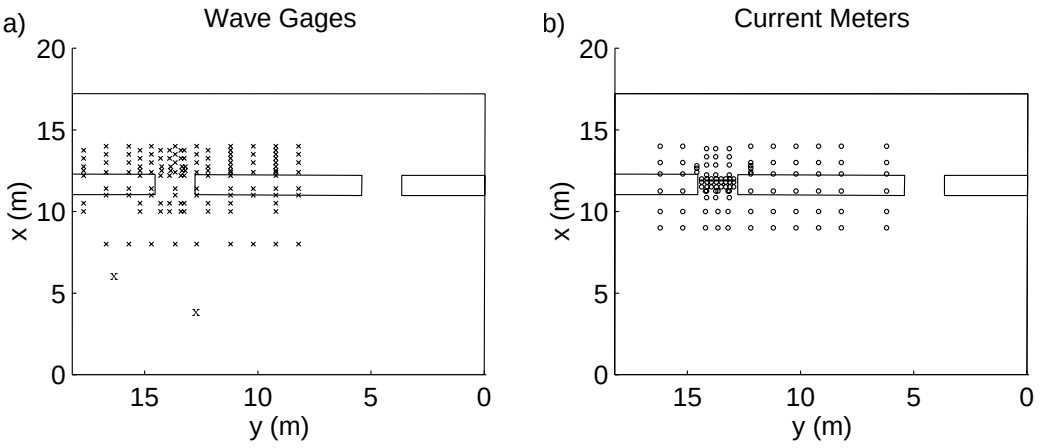


Figure 2: Sampling locations for ($a$) wave gages and ($b$) current meters.

Figure 2 shows the measurement locations for the 40 measuring runs described in this paper. The measurement locations were densely concentrated around one rip channel in order to resolve the strong pressure and velocity gradients near the rip current. However, measurements did span a large area of the basin and covered all regions of interest. The ADV measurements taken shoreward of x=10.85 m were taken 3 cm from the bottom. The offshore ADV measurement lines at x=10 m and 9 m were taken 4 cm and 5 cm from the bottom, respectively. The still water line was at x=14.89 m, the wave generator at x=0 m, and the water depth at the bar crest (x=12 m) was 3.6 cm.

## Results - Steady circulation

The waves were generated normally incident to the shoreline and the offshore wave height was 4.8 cm (at x=4 m, y=13.2 m) with a frequency of 1 Hz. The spatial variations of wave height and water level, time-averaged over the last

half of the data collection period (819 s), are shown in Figure 3. The measurements show that there is little variation in the mean quantities ($H_{rms}, \overline{\eta}$) offshore, but near x=12 m the wave height decays sharply due to strong breaking induced by the bar. Correspondingly, the intense wave breaking over the bar drives a sharp increase in the mean water level in this region and a wave-induced setup of ∼3 mm at the shoreline in the center of the basin (y=9.2 m). In the rip channel wave breaking is less intense and mostly occurs shoreward of x=12 m. Therefore there is a local elevation (hill) of wave height in the channel and the contours of $\overline{\eta}$ in the rip channel show a local depression (valley) trending in the offshore direction.

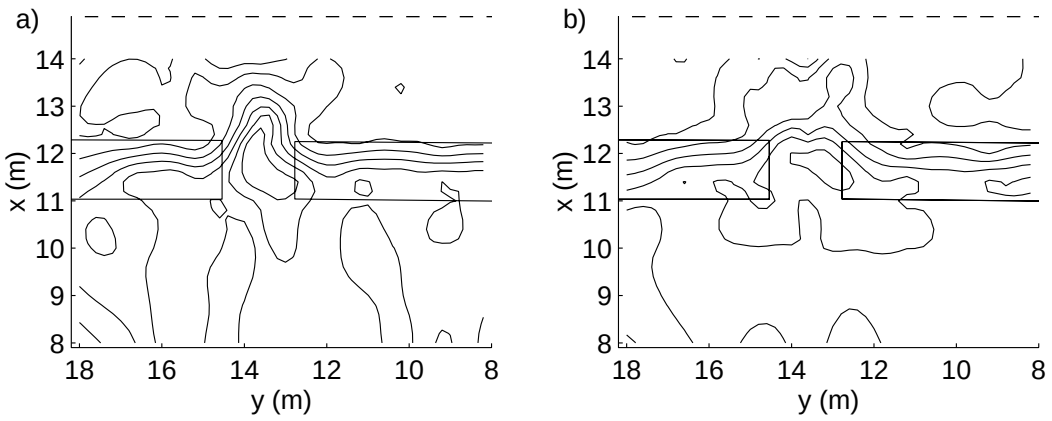


Figure 3: Contours of ($a$) $H_{rms}$ (contour interval = 0.5 cm) and ($b$) $\overline{\eta}$ (contour interval = 0.1 cm). $H_{rms}$ is computed from bandpassed ($0.03 < f < 5$ Hz) water surface elevation records.

Figure 4 compares the cross-shore variations of $H_{rms}$ and $\overline{\eta}$ measured through the rip channel and in the center of the basin. Notice the largest measured longshore gradients are near x∼ 12.3 m which is just shoreward of the bar in what would be considered the bar trough. It is also interesting to note that close to the shoreline at x=14 m, the longshore gradients are reversed from those in the trough.

The time average of the mean flows are shown in Figure 5. It can be seen that the longshore setup gradient induces strong longshore currents in the troughs which are driven towards the rip where they converge and exit offshore as rip currents. However, due to the reversal of the longshore setup gradient near the shoreline, the flow at the shoreline is driven away from the rip channels. Figure 5$a,b$ shows cross-shore profiles of the longshore currents measured near the rip channel and in the center of the basin (areas enclosed by dashed lines in 5$c$), respectively. There is very little longshore flow in the surf zone at the basin center which implies the dynamics are dominated by the cross-shore momentum balance in this region. Near the rip channel the longshore currents

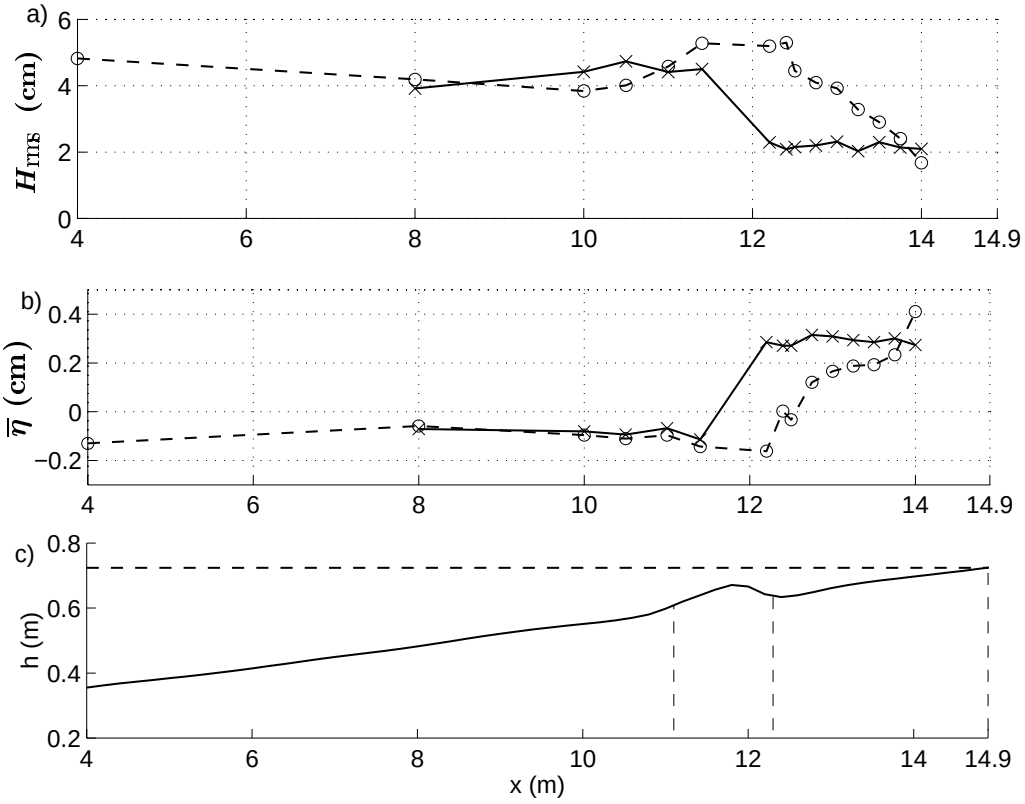


Figure 4: Cross-shore variation of $(a)$ $H_{rms}$ $(b)$ $\overline{\eta}$ measured in rip channel (dashed line) and in center of basin (solid line); $(c)$ cross-shore profile of bathymetry in center of basin.

are considerably stronger. Also, the reversal of longshore flow at the shoreline induces a pronounced shear on the shoreward face of the profile.

The entire measured circulation is shown in Figure 5$c$. The current vectors indicate that the dominant feature of the nearshore circulation is the strong offshore directed jet in the rip channel. In addition, there are two separate circulation patterns. The first is the classical rip current circulation which encompasses the longshore feeder currents at the base of the rip, the narrow rip neck where the currents are strongest, and the rip head where the current spreads out and diminishes. Offshore of the rip head the flow diverges and returns shorewards over the bars. The secondary circulation is the reverse flows just shoreward of the base of the rips. Here, the waves which have shoaled through the rip channels break again at the shoreline driving flows *away* from the rip channels which is opposite from the primary circulation.

Figure 6 shows the spatial variation of the time-averaged flows measured in the rip channel. At the entrance to the rip channel (6$a$,$b$) the rip current is a narrow offshore directed jet which is being fed by converging feeder currents

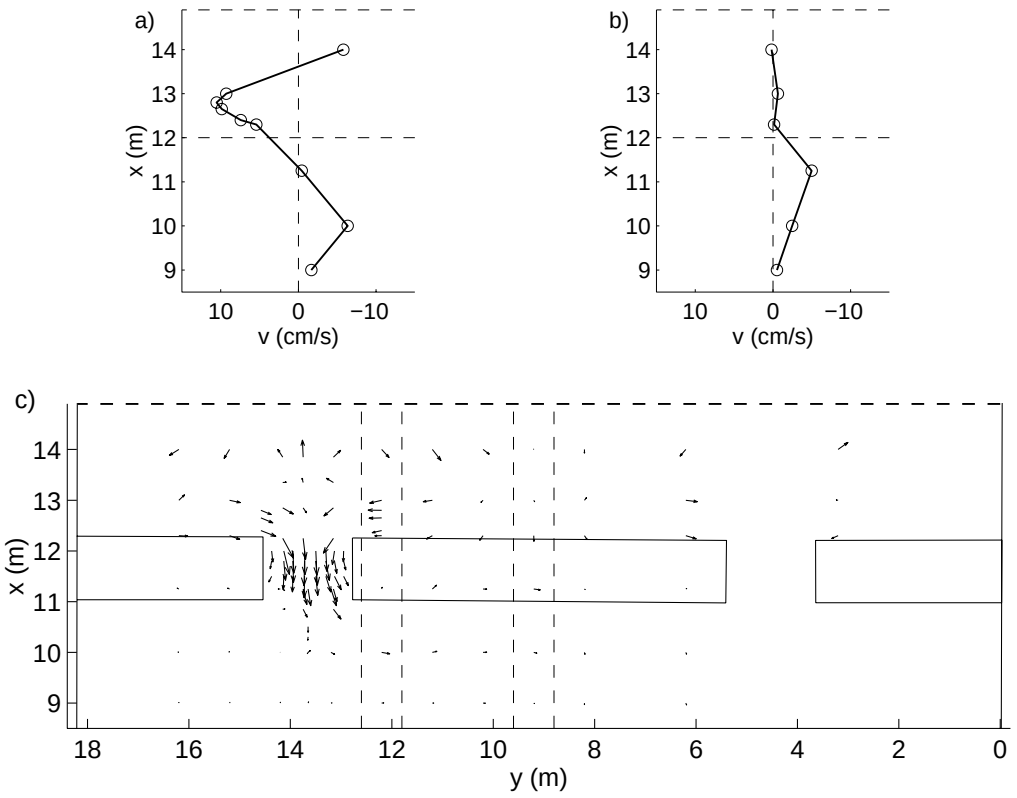


Figure 5: Cross-shore profiles of longshore current measured near ($a$) the rip channel, y=12.2 m, ($b$) the basin center, y=9.2 m. Measuring locations for ($a$) and ($b$) correspond to those enclosed by dashed lines in ($c$); ($c$) vectors of time-averaged measured current velocities. Dashed line at x=14.8 m represents still water line.

as shown by the opposite sign of the longshore velocity on each side of the rip. Figure 6$c,d$ shows that as the rip current exits the channel, the sign of the $v$ velocities has reversed which indicates the flow is starting to diverge. In addition, the offshore component of the flow, $u$, has a triangular longshore profile.

## Results - Unsteady currents

## Time scale 1

Visual observations obtained during the experiment indicated that, though a strong rip current was present in the rip channel throughout most of each experimental run, the entire rip current did migrate back and forth in the channel at slow time scales. The motion of the rip current could be easily followed by watching the narrow region of breaking waves on the rip neck as it moved back and forth in the channel.

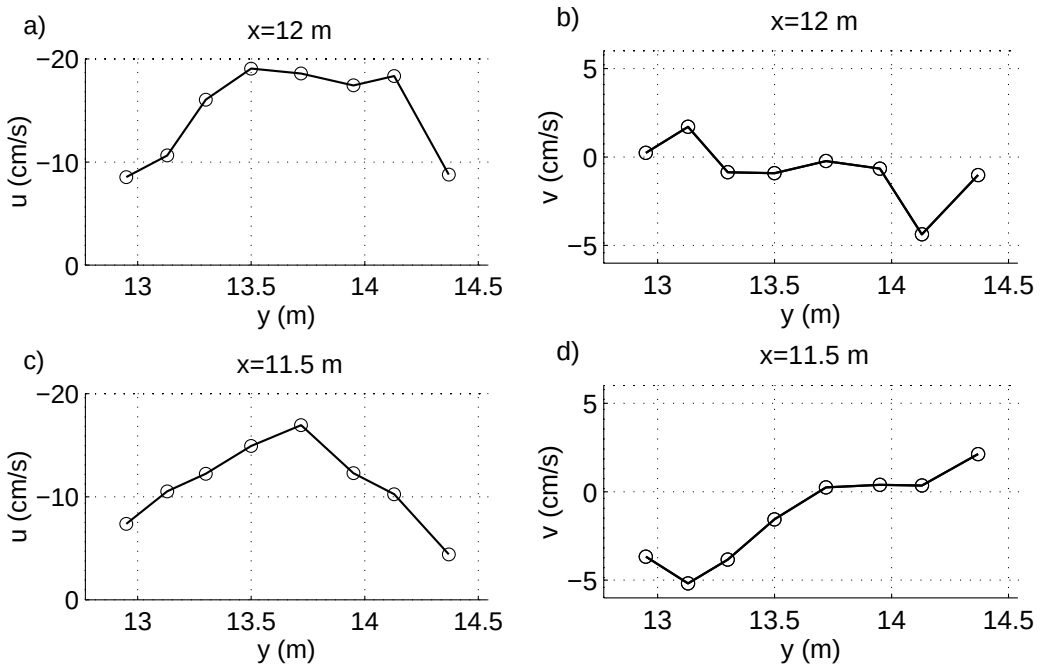


Figure 6: Time-averaged current profiles of cross-shore $(a,c)$ and longshore $(b,d)$ velocities measured in the rip channel.

Figure 7 shows time series of velocities measured in the rip channel. The raw time series of longshore velocity measured near the center of the rip channel is shown in Figure 7$a$. The time series shows strong oscillations in the longshore velocity at relatively long time scales, however, the record of cross-shore velocity taken at the same location does not show such dramatic fluctuations. Figure 7$b$ shows the lowpass filtered cross-shore velocity record. The filtered record is shown here in order to isolate the rip current flow from the strong oscillations at the incident wave frequency. The filtered record indicates that the offshore component of the rip remains relatively steady while the longshore component shows large oscillations between $+/-$ 25 cm/s. Spectral analysis of the longshore velocities shows an energy peak located near $f$=.007 Hz (Fig. 7$c$). This corresponds to a period of about 140 s, but, due to the finite length of the record, this estimate of the period should be considered approximate. However, this does suggest that motions of unusually low frequency (for lab scale) were present during the experiments.

Instantaneous profiles of the lowpass filtered ($f \leq 0.03$ Hz) currents measured near the entrance to the rip channel (x=12.25 m, y= 13.15, 13.75, 14.15 m) are shown in Figure 8. These profiles represent snapshots in time (with $\Delta t$=20 s) of the low frequency rip current motion. At time 1 (8$a$) the rip current is located on the right hand side of the channel as shown by the peak in the $u$ profile at y=14.15 m.

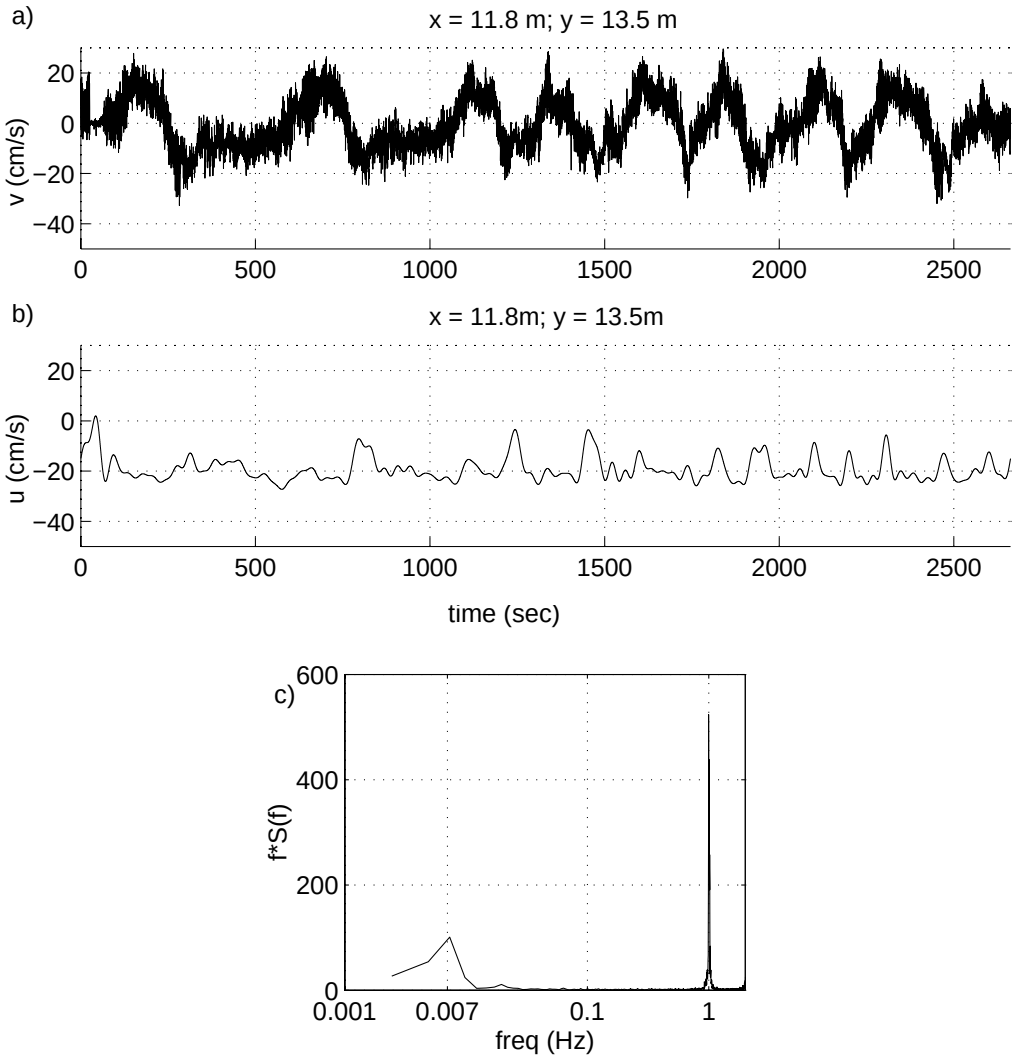


Figure 7: Time series of ($a$) longshore velocity and ($b$) lowpass filtered cross-shore velocity ($f \leq 0.03$ Hz) measured in rip channel; ($c$) frequency spectra computed from ($a$).

The profiles show the rip traversing the width of the channel in a span of 60 seconds. This 60 s time span represents one half of a rip migration period and explains the large oscillations in the longshore velocities with periods ∼140s. As the rip current migrates back and forth in the channel, a current meter located near the base of the rip is alternately immersed in opposite flowing feeder currents generating the large oscillations shown in Figure 7$a$.

Since the location of the rip current represents a local depression in the water level, the back and forth migration of the rip current is directly related to the mean water level gradients present in (or near) the rip channel. Figure

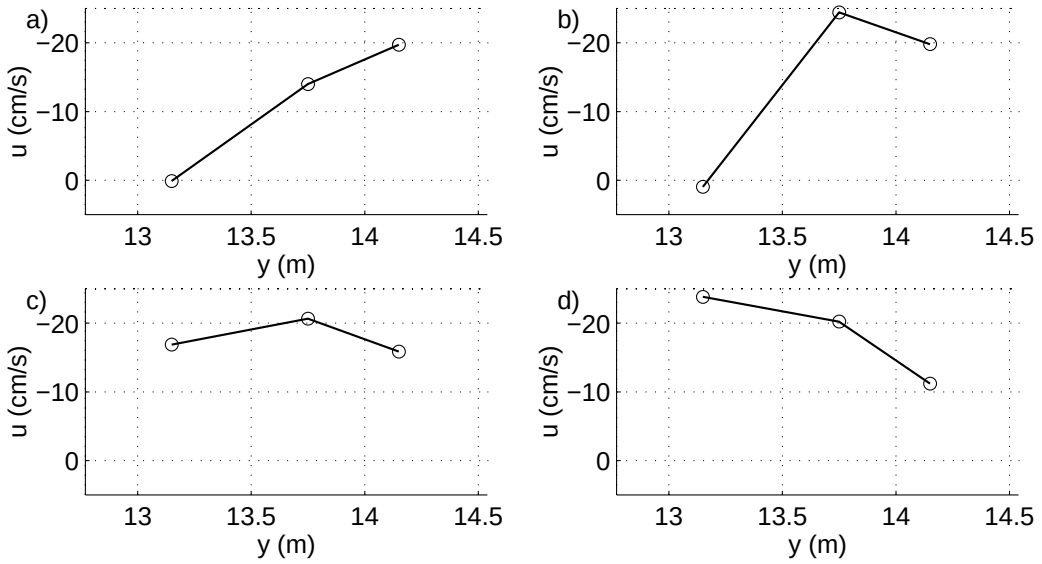


Figure 8: Snapshots of lowpassed $u$ records measured in rip channel at x=12.25 m, ($a$) t= 900 s, ($b$) t= 920 s, ($c$) t= 940 s, ($d$) t= 960 s.

$9a$-$c$ shows lowpass filtered time series of currents measured in the channel (x=12 m, y=13.95 m) with simultaneously measured water surface elevations (lowpass filtered) from two wave gages located at the sides of channel (x=12.2 m, y=13.25,14.3 m). Visual inspection of the time series shows that the large oscillations about zero seen in the longshore component of the rip current ($9a$) are well correlated with the direction of longshore water surface gradient indicated in $9c$. For example, at t=1400 s the lowpass filtered ($f \leq 0.03$ Hz) water surface elevation indicates a positive longshore (across the channel) gradient of $\sim$.004 while simultaneously the ADV located between the wave gages registers a strong negative longshore flow towards the depression. In the section of time series shown here the surface gradient and longshore current are seen to oscillate at periods ranging from $\sim$150-200 s. In contrast, the cross-shore component of the current ($9b$) is not dominated by oscillations at long periods and shows much weaker correlation with the observed surface gradient.

## Time scale 2

Near the exit of the rip channel the measured time series show oscillations of shorter time scale. Figure 10($a$ and $b$) shows time series (600 s duration) of longshore velocity and lowpass filtered cross-shore velocity, respectively, measured just offshore of the rip channel (x=10.85 m, y=13.75 m). It is evident from the records that during this time period the longshore velocities were dominated by motions at much shorter time scales than those shown in Figure $7a$. In fact, frequency analysis of the this section of the longshore

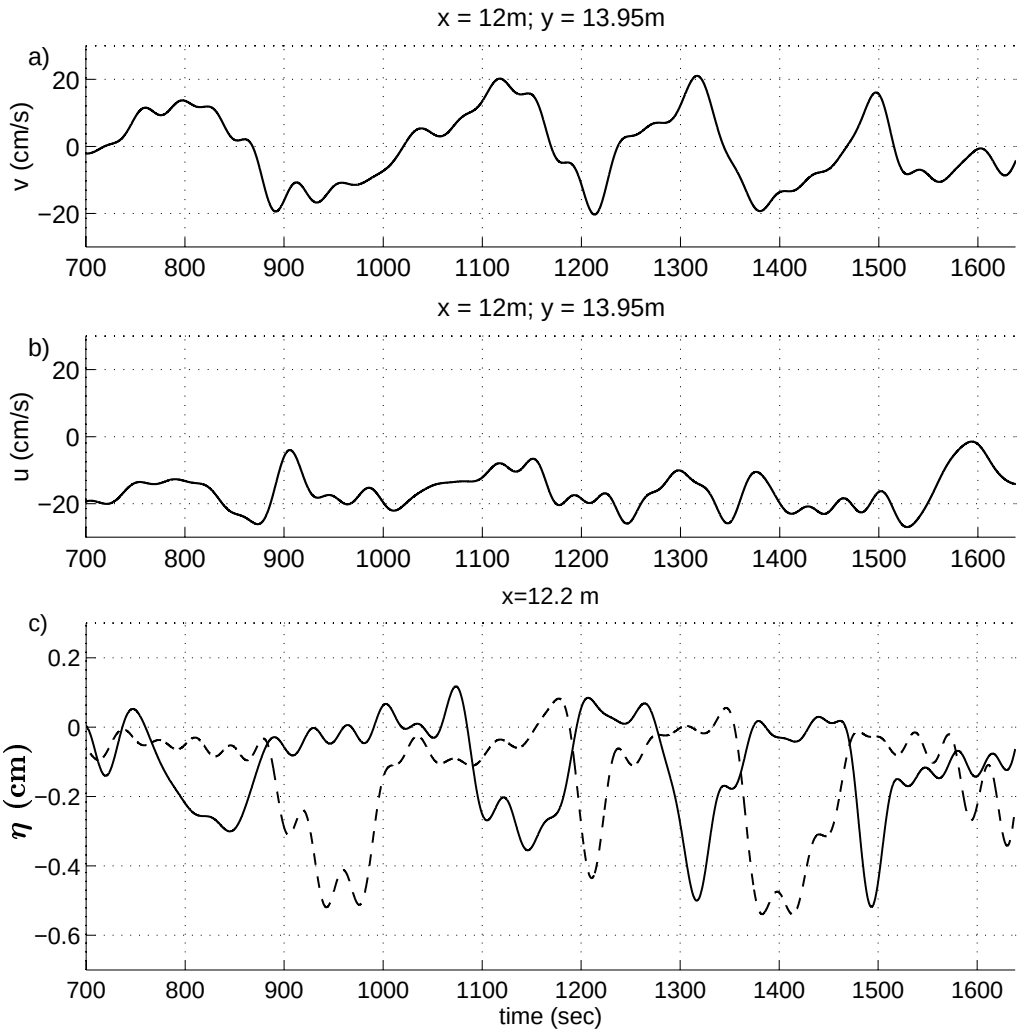


Figure 9: Lowpass filtered ($f \leq 0.03$ Hz) time series of ($a$) longshore velocity, ($b$) cross-shore velocity, and ($c$) water surface elevation measured near the entrance to the rip channel. Solid line in ($c$) corresponds to y=14.3 m, dashed line 13.25 m.

velocity record shows an energy peak near $f$=.06 Hz which corresponds to a period of ∼17 s. It is also interesting to note that Figure 10$b$ shows the increase of the offshore directed current (due to the rip migrating towards the ADV) occurs simultaneously with the onset of the short time scale oscillations in the longshore current. The strong correlation between the presence of a strong rip current and the generation of these short time scale oscillations suggests these oscillations are generated by an instability mechanism. Oscillations at this time scale are also seen in the unfiltered cross-shore record which is not shown here.

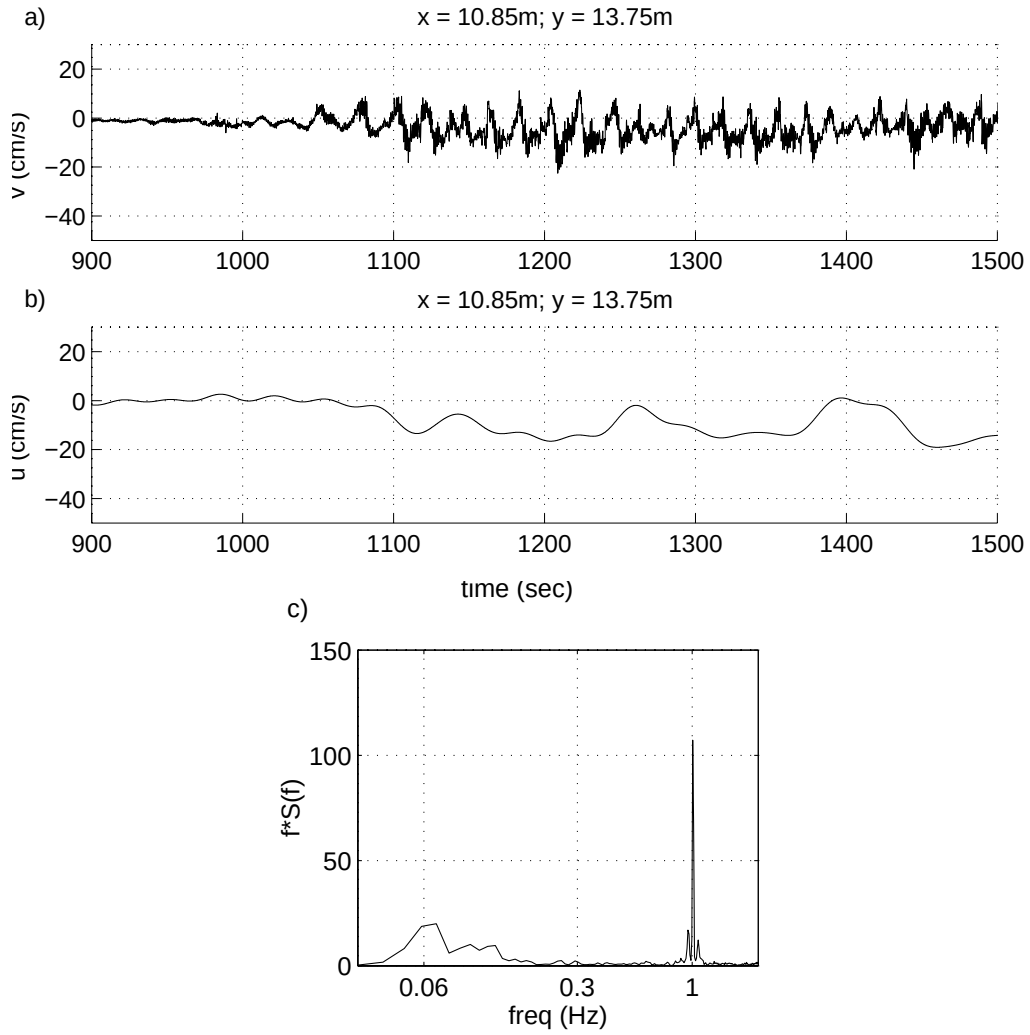


Figure 10: Time series of $(a)$ longshore velocity and $(b)$ lowpass filtered cross-shore velocity ($f \leq 0.03$ Hz) measured near exit of rip channel; $(c)$ frequency spectra computed from $(a)$.

The general features of the rip currents generated in this experiment are similar to narrow shallow water jets flowing into quiescent waters. Shallow water jets have been studied extensively by hydrodynamicists for more than a century and a well known phenomena associated with these jets is their tendency towards hydrodynamic instability. Therefore we can apply classical methods to model the experimental jets in order to determine if instability theory can describe the observed low frequency motions. We begin with the wave-averaged shallow water equations for x and y momentum and continuity:

$$u_t + uu_x + vu_y = -g\eta_x + \nu(u_{xx} + u_{yy}) - \tau_x \qquad (1)$$

$$v_t + uv_x + vv_y = -g\eta_y + \nu(v_{xx} + v_{yy}) - \tau_y \tag{2}$$

$$(uh)_x + (vh)_y = -\eta_t, \tag{3}$$

where subscripts denote partial differentiation (except for $\tau_x$, $\tau_y$) and the last two terms on the right-hand side represent viscous effects and bottom stress, respectively. By assuming a "rigid lid" ($\eta_t \approx 0$) and $h = h(x)$ we can combine the above three equations into the following vorticity equation:

$$\frac{D}{Dt}(\frac{u_y - v_x}{h}) = \frac{\nu}{h}\nabla^2(u_y - v_x) + \frac{1}{h}\left(\frac{\partial \tau_y}{\partial x} - \frac{\partial \tau_x}{\partial y}\right). \tag{4}$$

It is likely that viscous effects and depth variations play an important role in the dynamics of rip currents. However, the inclusion of these effects makes further analytical manipulation of the equations very difficult. Therefore, in order to gain estimates of the length and time scales of rip current instabilities, we will neglect the effects of viscosity and depth variability and, due to these simplifying assumptions, the resulting estimates should be considered to yield the correct order of magnitude. Applying the above mentioned assumptions reduces the vorticity equation to the following:

$$\frac{D}{Dt}(u_y - v_x) = 0. \tag{5}$$

We then assume the rip current can be represented by a steady offshore directed flow with superimposed small disturbances as:

$$\vec{u} = U(y) + \epsilon u(x, y, t) + \epsilon v(x, y, t). \tag{6}$$

The linearized equation governing the instabilities ($O(\epsilon)$) is then

$$\left(\frac{\partial}{\partial t} + U\frac{\partial}{\partial x}\right)(u_y - v_x) = -vU_{yy}. \tag{7}$$

If we define the velocities in terms of a stream function $\Psi(x, y, t)$ as $(u, v) = (-\Psi_y, \Psi_x)$ where $\Psi = \psi(y)\exp^{i(kx-\sigma t)}$ then we obtain from (7) the well-known Rayleigh stability equation,

$$(U - c)(\psi_{yy} - k^2\psi) = \psi U_{yy}, \tag{8}$$

where $c \equiv \sigma/k$ is the phase speed of the small disturbances (waves). The wave frequency $\sigma$ is allowed to be complex and modes with positive imaginary components will represent growing instabilities. In order to solve (8) we must specify the longshore profile of the mean flow $U(y)$. Here we choose a triangular jet profile since it is the simples representation. We then solve (8) for the unstable wavenumbers $k$ using a jet profile $U(y) = 20 - .8|y|$ (for $|y| \leq 25$;

$U(y) = 0$ otherwise). The width of the profile was estimated from visual observations using injected dye.

The predicted linear instability curve and dispersion relation are shown in Figure 11*a* and *b*. Figure 11*a* shows the most unstable wavenumber to be $k$= 4.9 rad/m which corresponds to a wavelength of ∼1.3 m and period of ∼16 s (from Fig. 11*b*). This wave period is remarkably similar to that determined from the data shown in Figure 10*a*. It should be noted, however, that the linear instability curve is very sensitive to the chosen mean rip current profile and the triangular profile we have used here is rather simplified. Nevertheless, the results do suggest that classical jet instability theory can explain some of the low frequency oscillations observed during this experiment.

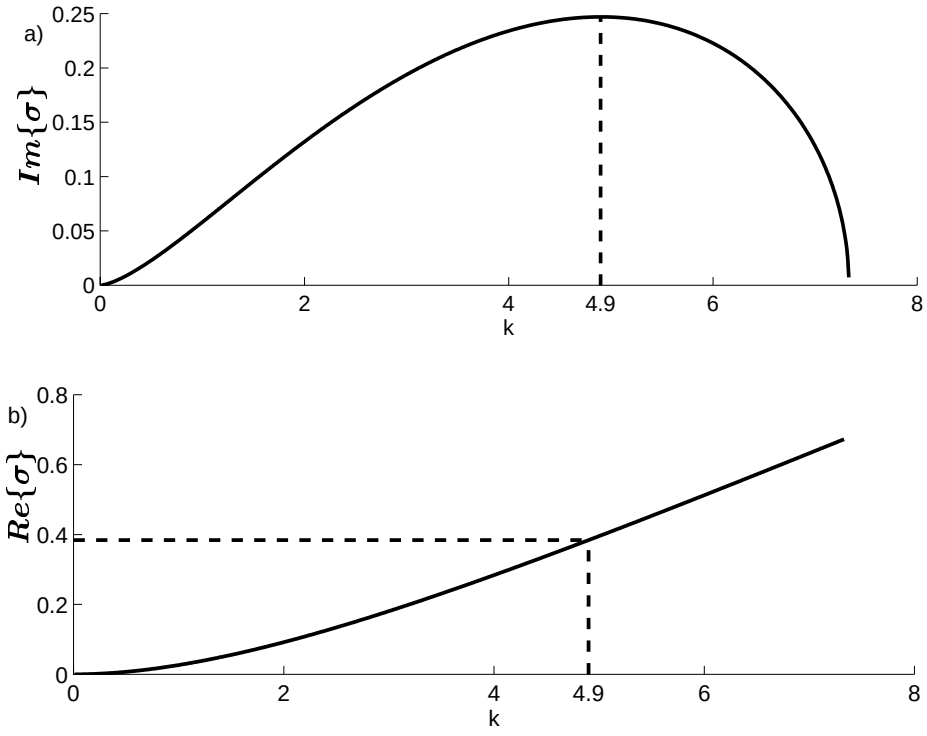


Figure 11: (*a*) Linear growth rate versus wavenumber for instabilities of a triangle jet (*b*) angular frequency versus wavenumber for the linear most unstable modes.

## Conclusions

Results from an experimental investigation into the dynamics of nearshore circulation in a rip current system have been presented. The results show that the nearshore circulation system is dominated by the forcing due to longshore variations in wave breaking. Strong breaking over the bar crest drives a longshore flow in the bar trough towards the rip channels where the flow is turned

offshore and exits the surf zone as a strong rip current. In addition, near the shoreline a secondary circulation exists which consists of flows driven away from the rip channels by the breaking of waves which have shoaled through the rip channel.

Analysis of the measured currents in the region of the rip channels shows that a significant amount of low frequency motion was present during the experiment. Very low frequency motion with periods greater than 100 s is shown to be the migration of the entire rip current back and forth in the channel. This motion was also evident in video records of the experiment which showed a narrow region of breaking waves, induced by the opposing rip current, moving back and forth in the channel. Sharp gradients in the measured water levels were observed to be associated with the rip currents. The rip current was located in a local depression in the water surface which also oscillated across the channel.

Low frequency motion with periods $\sim$17 s was also observed during the experiment near the exit of the rip channel. This motion was associated with the presence of a strong rip current and therefore was only intermittently present in a given current record due to the migration of the rip current away from a given ADV. This shorter time scale motion is distinct from rip current migration and is most likely instabilities (small vortices) generated by the strong shear flow. These instabilities are then advected along the rip from their generation point towards the rip channel exit. Applying a simplified shallow water instability model to the rip current and assuming a triangular jet profile shows that the model does remarkably well in predicting the scales of this motion. However, this must be considered somewhat fortuitous because of the many simplifications made in model. Nevertheless, it seems likely that this mechanism can account for much of the low frequency motion seen here.

## Acknowledgements

Funding for this research has been provided by ONR grant N00014-95-C-0075.

## References

Bowman, D., D. Arad, D. S. Rosen, E. Kit, R. Goldbery, and A. Slavicz, Flow characteristics along the rip current system under low-energy conditions, *Marine Geology,* 82, 149-167, 1988.

Haller, M. C., R. A. Dalrymple, and I. A. Svendsen, Experimental investigation of nearshore circulation in the presence of rip channels, (Abstract) *EOS Trans. AGU,* Vol.77, 46, 1996.

Haller, M. C., R. A. Dalrymple, and I. A. Svendsen, Rip channels and nearshore circulation, *Proc. of Coastal Dynamics '97,* ASCE, in press.

McKenzie, P., Rip current systems, *J. Geol.,* 66, 103-113, 1958.

Shepard, F. P., Undertow, rip tide or "rip current", *Science,* Vol. 84, 181-182, Aug. 21, 1936.

Shepard, F. P., K. O. Emery, and E. C. La Fond, Rip currents: a process of geological importance, *J. Geol.,* 49, 337-369, 1941.

Shepard, F. P. and D. L. Inman, Nearshore water circulation related to bottom topography and wave refraction, *Trans. Am. Geophys. Union,* 31, 196-212, 1950.

Short, A. D., Rip-current type, spacing and persistence, Narrabeen Beach, Australia, *Marine Geology,* 65, 47-71, 1985.

Sonu, Choule, J., Field observation of nearshore circulation and meandering currents, *J. Geophys. Res., 77,* 18, 3232-3247, 1972.

Tang, E. C.-S., and R. A. Dalrymple, Nearshore circulation: rip currents and wave Groups, in *Nearshore Sediment Transport Study* , R.J. Seymour ed., Plenum Press, 1989.